

AD-A228 046

COPY

ARO 23394.10-EG

(2)

# COMPRESSIBILITY EFFECTS ON DYNAMIC STALL OF OSCILLATING AIRFOILS

## FINAL REPORT

M. S. CHANDRASEKHARA & M. F. PLATZER

AUGUST 23, 1990

U. S. ARMY RESEARCH OFFICE

23394-EG

DEPARTMENT OF AERONAUTICS AND ASTRONAUTICS  
NAVAL POSTGRADUATE SCHOOL  
MONTEREY, CA 93943

DTIC  
ELECTED  
OCT 26 1990  
S B D  
*G*

APPROVED FOR PUBLIC RELEASE:  
DISTRIBUTION UNLIMITED.

90 14 9 0005

THE VIEW, OPINIONS, AND/OR FINDINGS CONTAINED IN THIS REPORT  
ARE THOSE OF THE AUTHORS AND SHOULD NOT BE CONSTRUED AS  
AN OFFICIAL DEPARTMENT OF THE ARMY POSITION, POLICY, OR DE-  
CISION, UNLESS SO DESIGNATED BY OTHER DOCUMENTATION

## REPORT DOCUMENTATION PAGE

1a. REPORT SECURITY CLASSIFICATION <u>Unclassified</u>		1b. RESTRICTIVE MARKINGS	
2a. SECURITY CLASSIFICATION AUTHORITY		3. DISTRIBUTION / AVAILABILITY OF REPORT Approved for public release; distribution unlimited.	
2b. DECLASSIFICATION/DOWNGRADING		4. PERFORMING ORGANIZATION REPORT NUMBER(S)	
5. MONITORING ORGANIZATION REPORT NUMBER(S) <i>ARO 23894.10-EG</i>		6a. NAME OF PERFORMING ORGANIZATION Naval Postgraduate School	
6b. OFFICE SYMBOL (If applicable) Code 67CH		7a. NAME OF MONITORING ORGANIZATION U. S. Army Research Office	
6c. ADDRESS (City, State, and ZIP Code) NAVA-NASA Joint Institute of Aeronautics Dept. of Aeronautics and Astronautics Monterey, CA 93943		7b. ADDRESS (City, State, and ZIP Code) P. O. Box 12211 Research Triangle Park, NC 27709-2211	
8a. NAME OF FUNDING/SPONSORING ORGANIZATION U. S. Army Research Office		9. PROCUREMENT INSTRUMENT IDENTIFICATION NUMBER <i>MIPR ARO 137-86</i>	
8c. ADDRESS (City, State, and ZIP Code) P. O. Box 12211 Research Triangle Park, NC 27709-2211		10. SOURCE OF FUNDING NUMBERS	
		PROGRAM ELEMENT NO.	PROJECT NO.
		TASK NO.	WORK UNIT ACCESSION NO.
11. TITLE (Include Security Classification) Compressibility Effects on Dynamics Stall of Oscillating Airfoils (Unclassified)			
12. PERSONAL AUTHOR(S) M. S. Chandrasekhara and M. F. Platzer			
13a. TYPE OF REPORT Final	13b. TIME COVERED FROM 4/86 TO 3/90		14. DATE OF REPORT (Year, Month, Day) 90/8/23
16. SUPPLEMENTARY NOTATION The view, opinions and/or findings contained in this report are those of the author(s) and should not be construed as an official Department of the Army position, policy, or decision, unless so designated by other documentation.			
17. COSATI CODES		18. SUBJECT TERMS (Continue on reverse if necessary and identify by block number) Unsteady Aeronautics, Dynamic Stall, Compressibility Effects, Schlieren Studies, LDV Methods for Unsteady Flows.	
19. ABSTRACT (Continue on reverse if necessary and identify by block number)  A research proposal to investigate the "Compressibility Effects on Dynamic Stall of Oscillating Airfoils" was submitted to ARO and the project was funded in April 1986. The aim was to obtain a basic understanding of the effect of compressibility on the phenomenon of dynamic stall under typical flight conditions encountered by a helicopter in forward flight, so that eventually a means for its control can be devised and thus, its flight envelope can be expanded.			
20. DISTRIBUTION/AVAILABILITY OF ABSTRACT <input type="checkbox"/> UNCLASSIFIED/UNLIMITED <input type="checkbox"/> SAME AS RPT <input type="checkbox"/> DTIC USERS		21. ABSTRACT SECURITY CLASSIFICATION Unclassified	
22a. NAME OF RESPONSIBLE INDIVIDUAL		22b. TELEPHONE (Include Area Code)	22c. OFFICE SYMBOL

angle of attack as:

$$\alpha = \alpha_0 + \alpha_m \sin \omega t$$

with the mean angle of attack  $\alpha_0$ , continuously variable from 0 to 15 degrees, the amplitude of oscillation  $\alpha_m$ , from  $2^\circ$  -  $10^\circ$  and the frequency from 0 - 100 Hz, in an oncoming flow Mach number M, from 0 - 0.5. The drive was installed in the FML in-draft wind tunnel at NASA Ames Research Center. Stroboscopic schlieren studies and interferograms as well as holographic interferometry studies were conducted for a wide range of flow conditions, amplitudes and frequencies. The results show that compressibility effects appear at  $M = 0.3$ , that a dynamic stall vortex forms for all Mach numbers, and that for  $M \geq 0.3$ , the dynamic stall angle decreases as M increases. On the other hand, increasing the degree of unsteadiness, i.e. increasing the reduced frequency, delays deep stall monotonically at all Mach numbers. Amplitude has a dominant effect, and dynamic stall occurs at lower angles of attack at lower amplitudes, yet this angle of attack is always higher than the static stall angle.

Interferometry studies have yielded some exciting new pictures of the density field around the leading edge, which are being currently analyzed.

## FINAL REPORT

1. ARO MIPR: 23394-EG

2. PERIOD COVERED BY REPORT: 1 April 1986 - 31 March 1990

3. TITLE OF PROPOSAL: Compressibility Effects on the Dynamic Stall of Oscillating Airfoils

4. NAME OF INSTITUTION: Naval Postgraduate School

5. AUTHORS OF REPORT: Prof. M.S.Chandrasekhara and Prof. M.F.Platzer

6. LIST OF MANUSCRIPTS SUBMITTED OR PUBLISHED UNDER ARO SPONSORSHIP DURING THIS REPORTING PERIOD, INCLUDING JOURNAL REFERENCES:

See next page.

7. SCIENTIFIC PERSONNEL SUPPORTED BY THIS PROJECT: The following personnel are partially supported by this project:

1. Prof. M.S.Chandrasekhara
2. Prof. M.F.Platzer
3. Dr. S.Ahmed (MCAT Institute, Contractor to NASA Ames Research Center)
4. Late Prof. S.Bodapati
5. Major R.R.Ryles. U.S. Army, M.S. 9/1987
6. Lt. S.D Hedrick. U.S. Navy, M.S. 12/1987
7. CPT.(P). B.E.Brydges. U.S. Army, M.S. 9/1989.

M.S.Chandrasekhara  
Department of Aeronautics and Astronautics  
Naval Postgraduate School  
Monterey, CA 93943

Accession For	
NTIS GRA&I <input checked="" type="checkbox"/>	
DTIC TAB <input type="checkbox"/>	
Unannounced <input type="checkbox"/>	
Justification	
By _____	
Distribution/	
Availability Codes	
Dist	Avail and/or Special
A-1	



## LIST OF PUBLICATIONS

1. M.S.Chandrasekhara and L.W.Carr. "Flow Visualization Studies of the Mach Number Effects on the Dynamic Stall of Oscillating Airfoils", *AIAA Paper No. 89-0023*, Jan. 1989. Also, *Jl. of Aircraft*, Vol. 27, No. 6, June 1990, pp. 516-522.
2. L.W.Carr, M.F.Platzer, M.S.Chandrasekhara, and J.A.Ekaterinaris, "Experimental and Computational Studies of Dynamic Stall", Presented at the *4<sup>th</sup> Symposium on Numerical and Physical Aspects of Aerodynamic Flows*, Jan. 1989. Also, Chapter 14, pp. 239 - 256, *Springer Verlag* 1990.
3. L.W.Carr and M.S.Chandrasekhara, "Design and Development of a Compressible Dynamic Stall Facility", *AIAA Paper No. 89-0647*, Jan. 1989. Also, to appear in *Jl. of Aircraft*.
4. M.S.Chandrasekhara, J.A.Ekaterinaris and L.W.Carr, "Experimental and Computational Tracking of the Dynamic Stall Vortex", *Bull. of Am. Physical Society*, Vol. 33, No.10, (1988), pp.2251.
5. M.S.Chandrasekhara and B.E.Brydges. "Amplitude Effects on Dynamic Stall of an Oscillating Airfoil". *AIAA Paper No. 90-0575*. Jan. 1990. Also submitted to *Jl. of Aircraft*.
6. M.S.Chandrasekhara, L.W.Carr, and S.Ahmed, "Comparison of Pitch Rate History Effects on Dynamic Stall", NASA/AFOSR/ARO Workshop on Physics of Forced Unsteady Separation, April 1990.
7. R.R.Ryles. "Investigation of Dynamic Stall Using LDV: Mean Flow Studies", *M.S. Thesis*, Naval Postgraduate School, Sep. 1990.
8. S.D.Hedrick, "Unsteady Flow field Measurements Using LDV", *M.S.Thesis*, Naval Postgraduate School, Dec. 1990.
9. B.E.Brydges, "Flow Visualization Studies of Dynamic Stall on an Oscillating

Airfoil", *M.S.Thesis*, Naval Postgraduate School, Sep. 1990

**Papers with partial support from ARO**

1. M.S.Chandrasekhara and L.W.Carr. "Design and Development of a Facility for Compressible Dynamic Stall Studies of a Rapidly Pitching Airfoil", Presented at *The 13<sup>th</sup> International Congress on Instrumentation of Aerospace Simulation Facilities*, Goettingen, West Germany, ICIASF 1989 Record, *IEEE Publication 89CH2762-3*

## **ACKNOWLEDGEMENTS**

This project was supported by the U.S. Army Research Office (ARO) under grant ARO-23394-EG to the U.S. Naval Postgraduate School (NPS) from April 1986- March 1990. It was monitored initially by Dr. R.E.Singleton and then by Dr. T.L.Doligalski. The funding was used to partially support the following personnel: Professor M.S.Chandrasekhara, Professor M.F.Platzer, Late Professor S.Bodapati, Mr. M.J. Fidrich (technician), Dr. S.Ahmed (through a subcontract to MCAT Institute, contractor to NASA Ames Research Center (ARC)), Major R.R.Ryles, CPT.(P) B.E.Brydges both of U.S. Army and Lt. S.D.Hedrick, U.S. Navy. The design support for the facility was provided by the Mechanical Systems and Controls Branch (Code EEE at NASA ARC) and the effort was partly funded by this grant. The above support is gratefully acknowledged.

Additional support was provided by the U.S. Naval Air Systems Command through their sponsorship of the direct funded research project at NPS and the Air Force of Scientific Research (AFOSR) and the Fluid Dynamics Research Branch, NASA Ames Research Center. The work was carried out in the Indraft Wind Tunnel of the Fluid Mechanics Laboratory (FML)at NASA ARC as a project of the Navy-NASA Joint Institute of Aeronautics. The support of Dr. S.S.Davis, Chief, Fluid Dynamics Research Branch and that of the FML staff is greatly appreciated.

Dr. L.W.Carr, U.S. Army AFDD was a co-operative participant in the project and provided his valuable expertise to this project on a continuing basis. His support and encouragement through out are gratefully acknowledged.

## SUMMARY

A research proposal to investigate the "Compressibility Effects on Dynamic Stall of Oscillating Airfoils" was submitted to ARO and the project was funded in April 1986. The aim was to obtain a basic understanding of the effect of compressibility on the phenomenon of dynamic stall under typical flight conditions encountered by a helicopter in forward flight, so that eventually a means for its control can be devised and thus, its flight envelope can be expanded.

The initial phase of the study was devoted to building a drive system to produce the necessary unsteady airfoil motion. A novel design was arrived at after reviewing the various possibilities and was built. It uses a four-bar chain mechanism of which the airfoil is one of the links. The drive can produce a sinusoidal variation of the angle of attack as

$$\alpha = \alpha_0 + \alpha_m \sin \omega t$$

with the mean angle of attack  $\alpha_0$ , continuously variable from 0 to 15 degrees, the amplitude of oscillation  $\alpha_m$ , from  $2^\circ - 10^\circ$  and the frequency from 0 - 100 Hz. in an oncoming flow Mach number M. from 0 ~ 0.5. The drive was installed in the FML indraft wind tunnel at NASA Ames Research Center. Stroboscopic schlieren studies and interferograms as well as holographic interferometry studies were conducted for a wide range of flow conditions, amplitudes and frequencies. The results show that compressibility effects appear at  $M = 0.3$ . that a dynamic stall vortex forms for all Mach numbers. and that for  $M \geq 0.3$ . the dynamic stall angle decreases as M increases. On the otherhand. increasing the degree of unsteadiness, i.e. increasing the reduced frequency, delays deep stall monotonically at all Mach numbers. Amplitude has a dominant effect. and dynamic stall occurs at lower angles of attack at lower amplitudes. yet this angle of attack is always higher than the static stall angle.

Interferometry studies have yielded some exciting new pictures of the density field around the leading edge, which are being currently analyzed.

## NOMENCLATURE

c	airfoil chord
f	frequency of oscillation, Hz
k	reduced frequency = $\frac{\pi f c}{U_\infty}$
M	free stream Mach number
$U_\infty$	free stream velocity
x	chordwise distance
$\alpha$	angle of attack
$\alpha_0$	mean angle of attack
$\alpha_m$	amplitude of oscillation
$\omega$	circular frequency, radians/sec

## 2. INTRODUCTION

The phenomenon of dynamic stall is very important in the field of helicopter aerodynamics. The present day helicopter flight envelope is severely restricted because of the adverse effects that are produced during dynamic stall, notably the excursions in the pitching moment associated with the streamwise movement of the dynamic stall vortex, with the result that its beneficial effects remain unharnessed. The problem of dynamic stall is well known and relates to the dynamic delay of stall by production of dynamic lift, when an airfoil is rapidly pitched past the static stall angle. Under such unsteady motion of the airfoil, a large dynamic stall vortex is produced with its origin near its leading edge and convects over it. The presence of the vortex contributes significantly to the dynamic lift, but the convection of the vortex towards the trailing edge results in severe dynamic loads on both the pilot and the helicopter, and hence, the aircraft controls are designed to restrict the vehicle from flying into those conditions. A comprehensive review of dynamic stall has been given

by Carr<sup>1</sup>. The phenomenon is very complicated due to its dependence on several factors namely, the airfoil shape, the leading edge geometry, the degree of unsteadiness (expressed in terms of the reduced frequency), free stream Mach number, Reynolds number, three dimensionality, the state of the boundary layer, the amplitude of the airfoil motion and mean angle of attack, etc. (McCroskey<sup>2</sup>). The process of dynamic stall is greatly affected by compressibility. Earlier experiments<sup>3</sup> have shown that the compressibility may even negate the benefits of dynamic stall. However, these early studies did not explore the problem completely. Some computational studies (Fung and Carr<sup>4</sup>, Ekaterinaris<sup>5</sup>) have shown that a supersonic flow region forms over the airfoil surface even at low Mach numbers. McCroskey et al<sup>6</sup> have shown that at a free stream Mach number as low as 0.2, the flow can develop high suction peaks leading to the formation of a local supersonic region. The consequent appearance of shock waves and their interaction with the boundary layer could have a dramatic effect on the dynamic stall process. It is very important to understand the basic physics of the process, so that eventually a means can be devised for its control and exploitation in real systems. This report describes an experimental effort that was carried out as a first step in this direction.

### **3. FACILITY, INSTRUMENTATION & TECHNIQUE**

#### **3.1. Description of the Drive System**

The experiments were conducted in the in-draft wind tunnel of the Fluid Mechanics Laboratory (FML) at NASA Ames Research Center (ARC). It is one of the ongoing dynamic stall research projects of the Navy-NASA Joint Institute of Aerodynamics between the Naval Postgraduate School and NASA ARC.

The details of the FML in-draft wind tunnel are given in Carr and Chandrasekhara<sup>7</sup>. The facility is one of a complex of 4 in-draft wind tunnels con-

nected to a  $108 \text{ m}^3/\text{sec}$  (240.00 CFM), 9.000 hp evacuation compressor. The test section size is 25.4cmX 35cm. X 100cm. The flow in the tunnel is controlled by a variable cross section downstream diffuser. Its throat is always kept choked so that no disturbances can propagate upstream from the other tunnels or the compressor into the test section.

A unique mechanism was designed and built to produce the oscillatory motion of the airfoil. It is described in Ref. 7. The drive system is located on top of the test section. The test section windows are connected to the drive and the sinusoidal movement of the windows results in an identical movement of the airfoil which is supported by the windows. The airfoil is supported by pins push fitted between two 2.54cm. thick optical quality glass windows. The airfoil supports are unique in that the pins carry the entire load. The pins are smaller than the local airfoil thickness and hence provide complete optical access to the airfoil surface. This makes detailed flow studies possible even at the surface.

The oscillating drive was designed to meet the following specifications:

$$\alpha = \alpha_0 + \alpha_m \sin 2\pi f t = \alpha_0 + \alpha_m \sin \omega t$$

$$0 \leq \alpha_0 \leq 15^\circ$$

$$2^\circ \leq \alpha_m \leq 10^\circ$$

$$0 \leq f \leq 100 \text{ Hz}$$

$$0 \leq M_\infty \leq 0.5$$

$$200,000 \leq Re \leq 10^6$$

$$\text{airfoil chord} = 7.62 \text{ cm.}$$

The airfoil chord and the flow conditions correspond to a helicopter in forward flight and the other conditions correspond to those of a  $\frac{1}{7}$ th scale model rotor, whose test results are directly applicable to a helicopter rotor.

Considerable effort was expended in designing a system capable of delivering the specifications. Special care was needed in the design to transfer the dynamic aerodynamic loads on the airfoil to the glass windows that support it. In view of the material properties of glass, special sleeves of delrin with wall thickness of  $2.54\mu m$  had to be custom machined and inserted between the glass and the pins that support the airfoil to cushion the direct loads on the glass. The drive system was carefully designed to maintain the same linkage ratio at all amplitudes and angles of attack so that the variation in the harmonic motion is always less than 0.1%. A flywheel system insures the constancy of the harmonic motion. The basic load pattern on the drive is cyclical and thus fatigue life became an important factor to be considered. The weakest elements in the system are the airfoil support pins. Other similar load bearing components include the bearing pins in the push rods, the pins connecting the windows to the push rods. The drive system and its weakest components were all designed for a fatigue life of  $10^7$  cycles at 100 Hz oscillation frequency. In view of the complex geometry of some of the components and loads on them, considerable effort had to be spent to develop a reliable design. The system is driven by an a.c. motor, which is connected to the drive by a transmission belt. All the design details are documented in an internal stress analysis report generated for the NASA ARC facility approval process. The facility with its drive system is referred to as the *Compressible Dynamic Stall Facility, (CDSF)*. Fig. 1 shows the CDSF.

### 3.2. Phase Locking Instrumentation

The CDSF is instrumented with 3 digital encoders. Of these, one is an absolute position encoder providing 3600 counts per revolution and is used for the mean angle of attack information. The other two are incremental position encoders with a resolution of 800 counts per revolution. One of the incremental encoders is used for obtaining the frequency/phase angle information. The other could be used for the

instantaneous angle of attack. But, for the series of experiments being reported, it was not used.

A triggering circuit was specially built for obtaining conditionally sampled data of the oscillating airfoil flow field. One of the modules in this circuit is a comparator, which compares the desired phase angle set as a BCD number corresponding to the appropriate encoder count with the changing encoder counts streaming into the module. When a match occurs, the circuit outputs a TTL pulse, which in turn triggers a light source for the schlieren studies or a laser for interferometry studies. The actual phase angle at which this occurs is immediately frozen on the display for documentation. No significant delays were noticed in the firing of the schlieren light source. However, when the laser was triggered by this means, the finite lasing time resulted in the actual phase angle being different from the selected number. To properly account for this, the circuit was modified to freeze the displays only when the laser flashes - by using a very sensitive photo diode that senses the laser light flash. In view of the different oscillating frequencies at which the airfoil was oscillated, the delay constantly changed. Hence, on-line calibration was performed for each frequency and amplitude of oscillation and the information was used appropriately. The trigger circuit also accommodates a display that indicates the frequency of oscillation and outputs this information for input to a computer.

Since detailed LDV studies are also planned, additional demands were placed on the phase locking circuitry by the random nature of the LDV data. Since the LDV data rate is dependent on particle arrival rate, which is in general random and depends upon the local flow, a means to read the instantaneous phase angles arises each time an LDV data sample is validated. This requires latching circuits to freeze the continuous encoder data based on an event in the flow- which is the appearance of co-incident LDV data in the U and V directions. Fig. 2 presents a schematic of the method followed. The LDV data is input to a NASA LDV multiplexer, to which the encoder outputs are also connected. The co-incidence detection pulse (i.e. the

data ready pulse) from the multiplexer is used to freeze the encoder data, until all the data is completely transferred to a microVAX II computer in the DMA mode. As soon as this is accomplished, the latches are released for fresh data. In view of the general paucity of the LDV data and the time it takes to transfer it to the computer, very high speed latches are needed both from reasonable experiment time and difficulty considerations. Such components have been used in this circuit. Fig. 3 shows a partial schematic of the circuit developed.

### 3.3. Details of Stroboscopic Schlieren Technique

The schlieren system used is standard and is shown in Fig. 4. It is also described in ref. 7 and 8. The phase angle at which the schlieren picture was desired was set as the corresponding encoder count on the front panel switches of the phase locking and triggering circuit as a BCD number. Pictures were then taken at this phase angle. A movie of the flow was also obtained for the case of  $M = 0.3$ ,  $k = 0.05$ ,  $\alpha = 10^0 + 10^0 \sin \omega t$ . To do this, another electronic circuit was designed to control the shutter of a stop-action camera for a set number of times. After the required number of frames for persistence were exposed, a different phase angle was selected and the process repeated through a complete cycle of oscillation.

### 3.4. Stroboscopic Dark Center Interferometry

*Dark Center Interferometry* is a technique which enables real time interferograms of the flow to be obtained. The real time aspect of the technique makes it a very attractive alternative to more conventional methods such as holography. The simpler requirements on the quality of the optical components makes it a preferred technique over the traditional Mach-Zehnder interferometry. However, its application to unsteady flow problems presents significant challenges both in terms of the requirements on the light source and on the recording equipment.

The technique uses nearly the same optical configuration as a schlieren system and is shown in Fig. 5. The optical components on the transmitting side of the system provide a parallel beam of light which has been expanded to fill the windows after spatially filtering it. The beam coming out of the test section is focussed to a spot on a transparent coated film strip. The coating on the film when exposed to the intense energy of the laser beam burns to create a dark spot, which blocks most of the light through it. This spot is created with no flow through the test section. When the flow is turned on, the deflection of the beam due to the density changes causes it to be focussed around the spot rather than on the spot itself. The diffracted light from around the spot and the little light passing through the spot itself then interfere resulting in a system of fringes in real time. The fringes satisfy all the relationships of the standard interferometry technique. Thus, a distribution of the flow density field results. By suitable fringe analysis techniques, the flow field quantities can be recovered.

When used for the oscillating airfoil dynamic stall flow field studies, after the creation of the spot, the flow was established and with the airfoil oscillating, pictures were obtained in a manner similar to the stroboscopic schlieren technique. As already stated, the laser was triggered at the desired phase angle of motion taking into account the appropriate delays and the displays were frozen when the light appeared.

### 3.5. Experimental Conditions

The matrix of experimental conditions for stroboscopic flow visualization is shown in Table 1. For selected conditions, real-time interferometry and LDV studies were also carried out. The results are discussed in the next section.

## 4. RESULTS AND DISCUSSION

The information presented below has been drawn from the various papers that resulted from the funding. As such, they are only briefly discussed and the original sources properly referenced. In cases where such a reference is still not available in open literature, more details are discussed.

### 4.1. Calibration

The calibration of the facility included the calibration of the wind tunnel and the encoders. The wind tunnel was always run with its variable cross section downstream throat choked to prevent any downstream disturbances from propagating upstream into the test section. The calibration process determined the range of the throat heights that are possible when a stable shock forms in the diverging portion of the diffuser. Further details can be found in Carr and Chandrasekhara<sup>7</sup>.

Calibration of the encoders was done by resting the airfoil on a machined block on which the airfoil surface was machined. The block could be set at different angles of attack by using precision wedges. The procedure consisted of recording the encoder counts for each of the angles. It should be noted that each angle of attack occurs twice during a cycle and the encoder was calibrated for both the upstroke and the downstroke of the airfoil motion. The data showed that the variation of angle of attack followed a sine wave. This can also be seen from Fig. 6 wherein the actual angle of attack variation has been read by a computer and plotted for a frequency of 20 Hz. and for the motion described by  $\alpha = 10^\circ + 10^\circ \sin \omega t$ .

### 4.2. Stroboscopic Schlieren Flow Visualization

Stroboscopic schlieren technique reveals the instantaneous density gradient picture of the flow, without any history effects in it. Each picture is a snap-shot of the

flow at the instant the picture is taken.

Fig. 7 presents a sequence of schlieren pictures for the case of  $\alpha = 10^\circ + 10^\circ \sin \omega t$  at a reduced frequency of 0.1 for  $M = 0.3$ . It should be noted that at low Mach numbers, the density gradients are small except near the leading edge. However, since the system used was very sensitive the flow details could be photographed.

The oncoming flow reaches stagnation at a point slightly below the leading edge, which appears as a dark region in all the frames in the figure around the leading edge. A movie taken for a similar condition (at  $k = 0.05$ ) clearly shows the downstream movement of the stagnation point on the pressure side of the airfoil as it pitches beyond an angle of attack of  $10^\circ$  during the upstroke. Eventually by  $\alpha \approx 13^\circ - 14^\circ$ , it settles down at  $\approx 3-5\%$  chord location.

As the airfoil pitches up, the flow around the leading edge accelerates and the suction peak develops. This region appears as a bright region, which terminates in another dark region on the upper surface. As the angle of attack increases further, the dark region grows and starts convecting downstream. Whereas the exact origins of the dynamic stall vortex could not be clearly determined, it is strongly believed to be in this region downstream of the suction peak where all the vorticity input due to the unsteady motion of the surface accumulates. By  $x/c = 10-15\%$ , the dynamic stall vortex becomes clearly visible as a tightly wound structure, for example at  $\alpha = 15.2^\circ$  in Fig. 7. At  $\alpha = 15.9^\circ$ , the gradients within the vortex begin to clearly appear as a sharp transition line separates the bright region from the dark region of positive density gradient. The flow is still bounded by the leading edge shear layer enveloping the vortex and the downstream flow is attached as can be seen at  $\alpha = 15.2^\circ$ , where the boundary layer downstream thickness has slightly increased. Further increase in the angle of attack causes the vortex to move downstream, while simultaneously thickening the boundary layer. Eventually, at  $\alpha = 18.1^\circ$ , the vortex is shed and deep stall occurs. The airfoil generates lift till this angle of attack, which is substantially higher than the static stall angle of  $12.4^\circ$ . Beyond the deep stall angle, the flow is

completely separated from the leading edge, three dimensional, and highly turbulent, with a large wake. As the airfoil pitches down, reattachment occurs at considerably below the static stall angle. In the figure, it can be seen that even at  $\alpha = 8.4^\circ$ , the process is not complete. The movie also shows the highly turbulent region as deep stall occurs and as the airfoil reaches the top of the cycle.

Similar features were observed at most Mach numbers, reduced frequencies and amplitudes. Chandrasekhara and Carr<sup>8</sup>, Carr et al<sup>9</sup>, Chandrasekhara and Brydges<sup>10</sup>, and Brydges<sup>11</sup> provide these details.

#### 4.3. Shock Formation over the Airfoil

There is a general consensus among researchers that the rapid airfoil movement generates such strong suction pressures that the local flow becomes supersonic and eventually the flow returns to the subsonic state via a shock. Computational studies by Fung and Carr<sup>4</sup> have pointed to shock formation. However, it has remained a postulate till now and has never been directly verified experimentally. Fig. 8a shows the first such documentation of a shock in the flow at  $M = 0.45$ ,  $k = 0.075$  and  $\alpha = 10^\circ + 2^\circ \sin \omega t$  at  $\alpha = 9.1^\circ$ . The shock is located at  $x/c \approx 7\%$  and is about 1.5% high. Although its position is unsteady, the above numbers reasonably quantify the shock features. It remains on the surface till  $\alpha = 9.6^\circ$ , when it breaks down. Fig. 8b clearly shows that the breakdown occurs as a  $\lambda$  shock, indicating the laminar nature of the flow. Generally, no shock induced separation could be found, but occasionally a thin shear layer seemed to separate when the shock moved into the dark region downstream. At the condition tested, it was a highly intermittent phenomenon and could not be properly documented due to the synchronizing problems. However, a visual observation showed that it was occurring occasionally and it is schematically depicted in Fig. 8c. It is hoped that further experiments with a high speed camera will allow capturing of this event properly.

#### 4.4. Effect of Mach Number

The primary emphasis of this research is the study of the compressibility effects on dynamic stall. This effect was assessed in two ways. Firstly, the dynamic flow field pictures were compared at different Mach numbers, at the same reduced frequency, when the dynamic stall vortex was approximately at 50% chord location. Such a qualitative comparsion is shown in Fig. 9 (from ref. 8). It can be seen that for  $M \leq 0.3$ , the angle of attack at which the vortex reaches  $x/c = 0.5$  is  $15.1^\circ$  and independent of Mach number. For  $M \geq 0.3$ , the corresponding angle of attack decreases progressively from  $13.8^\circ$  at  $M = 0.35$  to  $12.3^\circ$  at  $M = 0.45$ , indicating strong effects of compressibility beyond  $M = 0.3$ . Thus,  $M = 0.3$  can be considered to be the delineating Mach number for compressibility effects. These results were quantified by following the dynamic stall vortex center location over the airfoil surface with increasing angle of attack. The results are shown in Fig. 10 for a reduced frequency of 0.05. The airfoil angle of attack is plotted as a function of the chordwise location of the vortex in it. It is clear that within the experimental scatter and the subjectivity of such an approach, the vortex behavior appears identical till  $M = 0.3$ . Beyond this, dramatic changes can be seen as the vortex begins to appear earlier in the pitching cycle, i.e. at lower angles of attack as  $M$  increases. Thus, deep dynamic stall also occurs at lower angles of attack as the Mach number is increased. This result leads to the conclusion that compressibility promotes the dynamic stall process.

#### 4.5. Effect of Reduced Frequency

The effect of increasing the reduced frequency (or the degree of unsteadiness) is shown in Fig. 11 wherein once again the vortex center location is plotted as a function of angle of attack for different Mach numbers. The curves for larger  $k$  are higher indicating that as the reduced frequency increases, the vortex remains closer

to the leading edge at higher angles of attack. Thus, the deep stall angle steadily increases as  $k$  increases. For example, at  $M = 0.3$ , the deep stall angle is  $15.9^\circ$ , and for  $k = 0.1$ , it is  $18.1^\circ$ . This result is true even at higher Mach numbers, and in the compressibility range. Even though it was seen from the previous section, that increasing Mach number promotes stall, increasing  $k$  has the opposite effect at all Mach numbers. This is due to the fact that the vorticity generated by the airfoil motion is larger at higher  $k$  and thus is available for the vortex. This additional vorticity enables the airfoil to produce lift till higher angles of attack until the vortex is shed. Thus, increasing  $k$  alleviates dynamic stall. Ref. 8 and 9 provide additional results.

#### 4.6. Effect of Amplitude

One of the issues still largely unknown in dynamic stall is the effect of the amplitude of unsteady motion. McCroskey<sup>6</sup> states that the effect is large. To assess this effect in general and in particular when compressibility effects are present, experiments were conducted at amplitudes of  $2^\circ$ ,  $5^\circ$  and  $10^\circ$ . Ref. 9 describes the results of this study in detail and the salient features are summarized below. Fig. 12 presents the effects at different Mach number and reduced frequencies. In all these, the uppermost curve is for the largest amplitude of  $10^\circ$  and the lower most curve is for the  $2^\circ$  amplitude. It is evident that at larger amplitudes, stall is delayed to higher angles of attack. This is a somewhat surprising result because, for example, at  $\alpha_m = 5^\circ$ , for  $M = 0.35$ , the dynamic stall angle is  $12.9^\circ$ , whereas for  $\alpha_m = 10^\circ$ , it is  $15.2^\circ$ . One expects that the flow at the lower amplitude would be still attached at  $15.2^\circ$  because the degree of unsteadiness is the same in both cases. However, on further analysis, it becomes clear that the flow is subjected to a much larger surface acceleration at the larger amplitudes. Also, the local flow pressure gradients are larger for the larger amplitudes because of the motion history, for motion starting from the same mean

angle. Thus, the total amount of vorticity generated is larger at the larger amplitudes leading to the conclusion that such flows can sustain greater pressure gradients and thus, the vortex remains over the surface. The result appears to be valid both in the incompressible and compressible flow regimes. It is also interesting to point out that the dynamic stall vortex still formed for all cases studied, even though in some cases, the maximum angle of attack reached is still below the static stall angle. Such a case is shown in Fig. 12 where the vortex has just formed very near the top of the cycle for the case of  $\alpha = 10^0 + 2^0 \sin \omega t$  at  $M = 0.35$ .

#### 4.7. Interferometry Studies

Fig. 13 presents one of the several interferograms obtained for the oscillating airfoil. The experimental conditions for this are  $M = 0.45$ ,  $k = 0.05$ ,  $\alpha = 10.32^0$  and the angle of attack was varied as  $\alpha = 10^0 + 10^0 \sin \omega t$ . The stagnation region can be seen on the lower surface at  $\approx 2 - 3\%$  chord location. In the accelerating flow from here, the presence of a strong suction can be inferred from the closely spaced fringes and the Mach number is increasing rapidly. A large cell of accelerating flow forms at  $x/c \approx 6 - 7\%$ , where the local Mach number reaches about 0.8 in the last discernible fringe. The shear layer underneath the cell shows a large number of fringes as the outer flow merges with the boundary layer. A closer examination of the shear layer reveals the curvature of the fringes, indicating that dynamic stall has already started.

The inset in the figure provides additional details of the flow near the leading edge. The large number of fringes in this region once again indicates that the density (and pressure) gradients are significant here. Currently, software and algorithms are being developed for improving the fringe quality digitally and to provide automated analysis so that these details can be recovered from the large number of interferograms obtained.

#### 4.8. LDV Studies

LDV studies have begun for obtaining the velocity data of the streamwise and vertical components of velocity in the dynamic stall flow field. In addition to the complexities described in the section on instrumentation, there are the complications arising from the requirements of proper seeding and the fact that close to the airfoil, blockage of the beams occurs during part of the oscillation cycle and hence no data exists. Further, owing to the fact that the measurements are being made of the unsteady flow field, a large number of samples have to be collected to arrive at a meaningful ensemble average at each of the desired phase angles. Typically, the data shown in Fig. 14 were obtained from 10,000 samples in each of the velocity channels (along with the phase positions). The data were sorted into 36 bins by software developed specially for this experiment and the averages computed for each bin. The software package is very comprehensive and incorporates several features for data validation, binning, curve fitting with a Fourier series of variable number of terms so that data in missing bins can be interpolated, histogram plotted etc. Data acquisition is ongoing with a nominal flow grid involving 20 midspan vertical points at 20 streamwise stations amounting to a total of 4 million samples. Given the random nature of LDV data and the fact that the valid data (coincident data in both the U and V channels) rate is generally poor, ranging from a few to a few hundred (400 at best) per second, the experiments are very time consuming and difficult. Nevertheless, the effort has proceeded reasonably successfully as can be seen from Fig. 14 obtained for  $M = 0.3$ ,  $k = 0.05$  and  $\alpha = 10^\circ - 10^\circ \sin \omega t$ , at  $x/c = 0.0$ ,  $y/c = 0.167$ ,  $z/c = 0.0$ . The streamwise velocity varies from about 115 m/s to 145 m/s as the phase angle from 0 degrees ( $\alpha = 10^\circ$ ) to  $\approx 210^\circ$ . At  $\alpha = 0^\circ$ , i.e. when the phase angle is 90 degrees, the flow velocity reaches the free-stream velocity corresponding to  $M = 0.3$  and then rises to its maximum value as the airfoil pitches up. The velocity drops rapidly to  $\approx 95$  m/s at a phase angle of about 215 degrees, which corresponds to the

dynamic stall angle of about  $15.9^{\circ}$  as determined from the schlieren studies. (see Table 2). This agreement is very good. The velocity recovers to the 0 degree phase value as the airfoil returns to its mean angle of attack. A corresponding variation in the vertical velocity can also be seen with its minimum at  $90^{\circ}$  phase, ( $\alpha = 0^{\circ}$ ). As the stall angle approaches, the vertical velocity component rises dramatically following the separating leading edge streamline. Once again, as the airfoil returns to its mean angle of attack, the flow reattaches and the vertical velocity drops to the zero phase angle value. Measurements at other locations in the flow field show that the flow is affected at large distances from the airfoil indicating the strong interactions that exist between the inner viscous and the outer inviscid regions. These are the first set of dynamic stall velocity data obtained with non-intrusive optical instrumentation and it is hoped that in a very short while, the substantial velocity data base that is currently being generated will lead to some new ideas about the flow field.

## 5. CONCLUSIONS

The study has led to the following major conclusions:

1. A dynamic stall vortex is present at all Mach numbers.
2. Compressibility has a significant effect on the dynamic stall process. The delineating Mach number between the incompressible and compressible flow regimes is 0.3. Stall is promoted by increasing the Mach number above this value.
3. A shock is present on the airfoil in the region  $0 \leq \frac{x}{c} \leq 7\%$  for certain flow conditions.
4. Increasing reduced frequency alleviates the stall process.
5. Increasing the amplitude results in the dynamic stall being delayed to higher angles of attack. At all amplitudes, Mach number and reduced frequency have similar effects.
6. Interferometry studies indicate strong gradients within the dynamic stall

vortex. The local Mach number has been estimated to reach a value as high as 0.8 at a free stream Mach number of 0.45.

7. The leading edge region supports a number of fringes in the interferograms, pointing to the large suction peaks and accelerations there.

8. LDV studies offering the first velocity data in the dynamic stall flow field under compressibility conditions have been obtained.

Further analysis of all the results is under way presently.

## 7. REFERENCES

<sup>1</sup> Carr, L.W., "Progress in Analysis and Prediction of Dynamic Stall," *Journal of Aircraft*, Vol. 25, No.1, Jan. 1988, pp. 6-17.

<sup>2</sup> McCroskey, W.J., "The Phenomenon of Dynamic Stall," NASA TM 81264, March 1981.

<sup>3</sup> Harper, P.W. and Flanigan, R.E., "The Effect of Change of Angle of Attack on the Maximum Lift of a Small Model," NACA TN 2061, March 1950.

<sup>4</sup> Fung, K.Y. and Carr, L.W., "An Analytical Study of Compressibility Effects on Dynamic Stall," *Proceedings of the 1<sup>st</sup> National Fluid Mechanics Conference*, Part 2, pp. 799-805, 1988.

<sup>5</sup> Ekaterinaris, J.A., "Computational Studies of Dynamic Stall," AIAA Paper No. 89-0024, Jan. 1989.

<sup>6</sup> McCroskey, W.J., McAlister, K.W., Carr, L.W., Pucci, S.L., Lambert, O. and Indergrand, R.F., "Dynamic Stall on Advanced Airfoil Sections," *Journal of American Helicopter Society*, July 1981, pp. 45-50.

<sup>7</sup> Carr, L.W. and Chandrasekhara, M.S., "Design and Development of a Compressible Dynamic Stall Facility," *AIAA Paper No. 89-0647*, Jan. 1989. Also,

submitted to *Jl. of Aircraft*.

<sup>8</sup> M.S.Chandrasekhara and L.W.Carr, "Flow Visualization Studies of the Mach Number Effects on the Dynamic Stall of Oscillating Airfoils", *AIAA Paper No. 89-0029*, Jan. 1989. Also, *Jl. of Aircraft*. Vol. 27, No. 6, June 1990, pp. 516-522.

<sup>9</sup> Carr, L.W., Platzer, M.F., Chandrasekhara, M.S. and Ekaterinaris, J.A., "Experimental and Computational Studies of Dynamic Stall", *Proceedings of the Fourth Symposium on Numerical and Physical Aspects of Aerodynamic Flows*, Springer Verlag, 1989, Chapter 14.

<sup>10</sup> M.S.Chandrasekhara, and B.E.Brydges, "Amplitude Effects on Dynamic Stall of an Oscillating Airfoil", *AIAA Paper No. 90-0575*, Jan. 1990. Also submitted to *Jl. of Aircraft*.

<sup>11</sup> B.E.Brydges, "Flow Visualization Studies of Dynamic Stall on an Oscillating Airfoil", *M.S.Thesis*, Naval Postgraduate School, Sep. 1990.

**TABLE 1: EXPERIMENTAL CONDITIONS**

M	K						
	0	0.0125	0.025	0.050	0.075	0.100	0.150
0.15			X		X	X	X
0.20	S	X	X	X	X	X	X
0.25	S	X	X,Y	X,Y	X,Y	X,Y	X,Y
0.30	S	X	X,Y,Z	X,Y,Z	X,Y,Z	X,Y,Z	X,Y,Z
0.35	S		X,Y,Z	X,Y,Z	X,Y,Z	X,Y,Z	Y
0.40	S		X,Y,Z	X,Y,Z	X,Y,Z	Y,Z	Z
0.45	S		X,Y,Z	X,Y,Z	X,Y,Z	Y,Z	

S: Steady flow  
 X: 10 deg. amplitude  
 Y: 5 deg. amplitude  
 Z: 2 deg. amplitude

**TABLE 2: VORTEX RELEASE ANGLES OF ATTACK**

M	k						
	0	0.0125	0.025	0.050	0.075	0.100	0.150
0.15						18.1	19.5
0.20				15.9	17.1	18.3	
0.25	13.8	14.5	15.9	17.1	18.1		
		13.7	13.9	14.4	14.6		
0.30	12.4	13.4	14.1	15.9	17.6	18.1	
			13.3	14.1	14.3	14.6	
0.35	11.6	13.8	15.2	15.9	13.8	14.1	
		12.3	12.9		11.9	11.98	
0.40	10.8	13.1	14.5				
		11.9	12.3		12.9		
		11.2			11.6	11.7	
0.45	9.5	12.3	14.2		12.6		
		11.2	11.9		10.8	11.4	

First row: 10 deg. amplitude  
Second row: 5 deg. amplitude  
Third row: 2 deg. amplitude

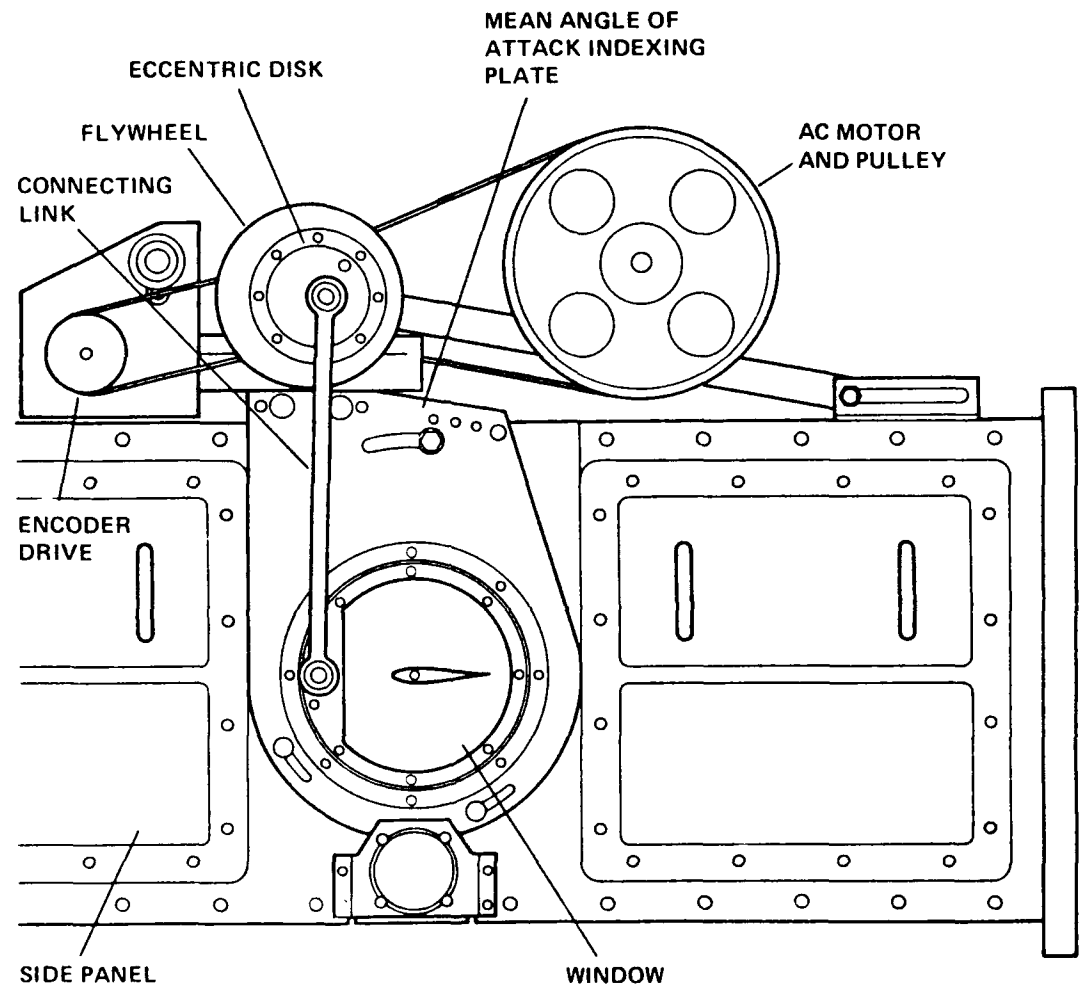


Fig. 1. Schematic of the Compressible Dynamic Stall Facility

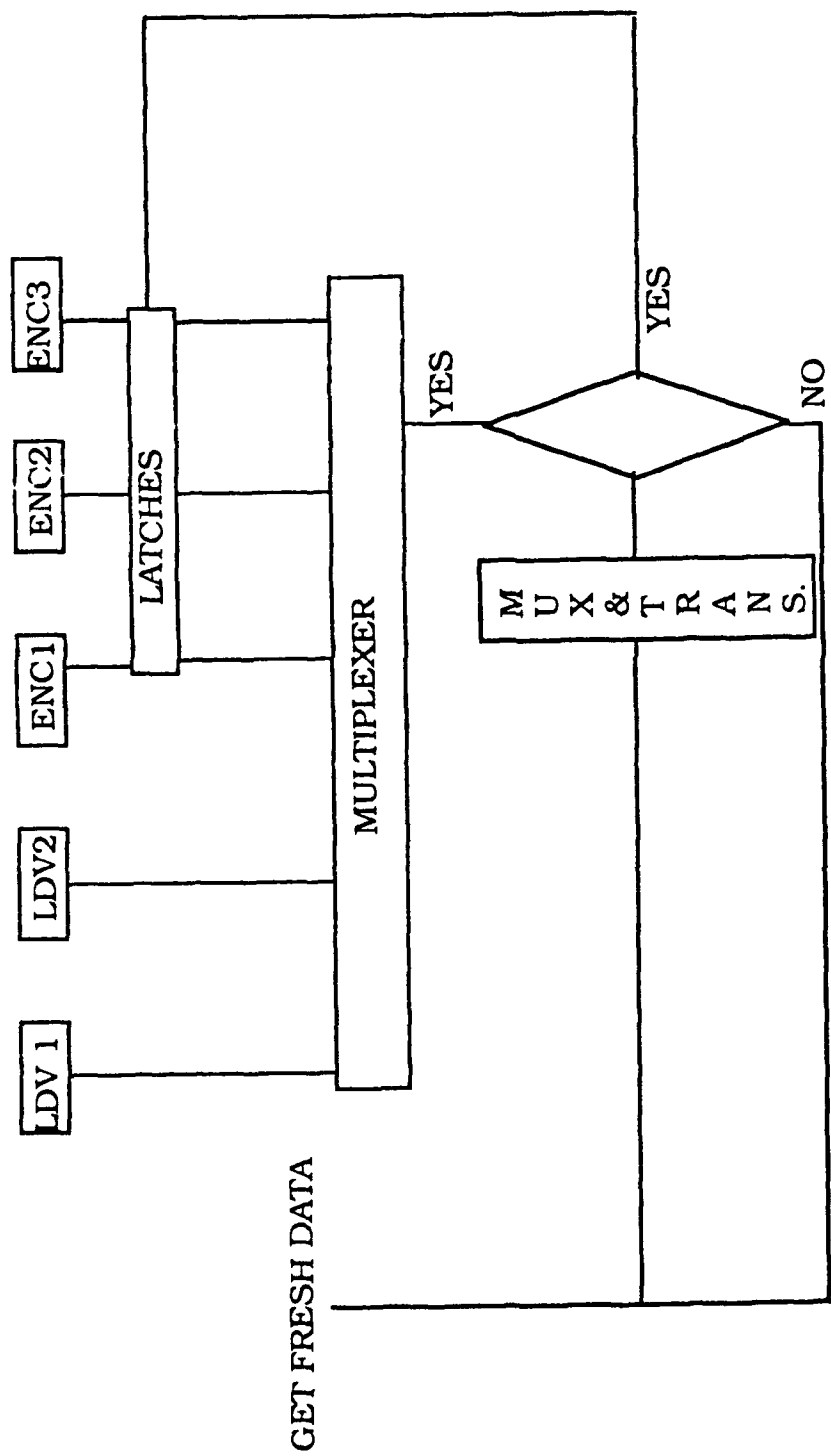


Fig. 2. Schematic of the LDV Data Acquisition Method

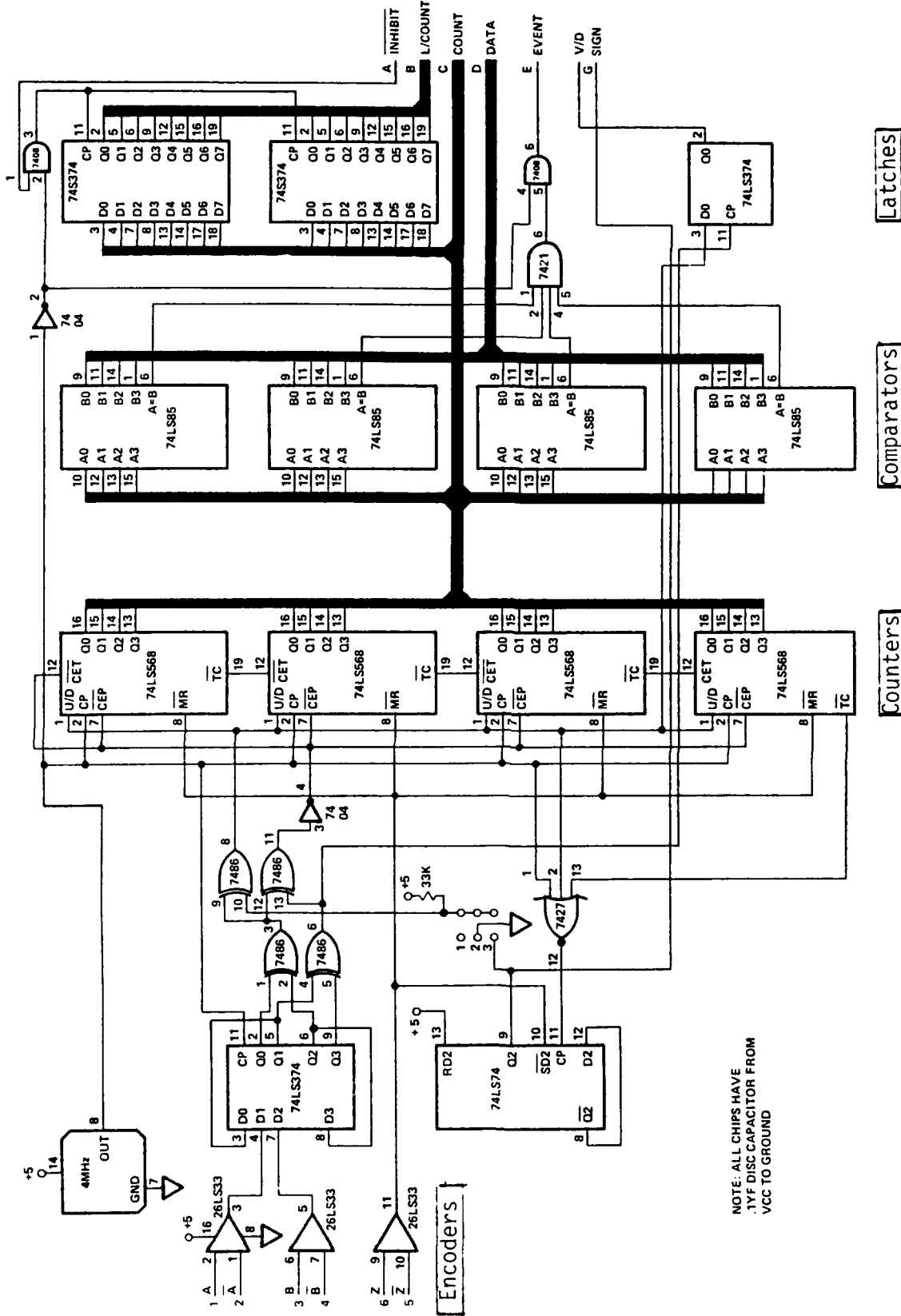


Fig. 3. Partial Schematic of the Phase Locking and Triggering and Triggering Circuit

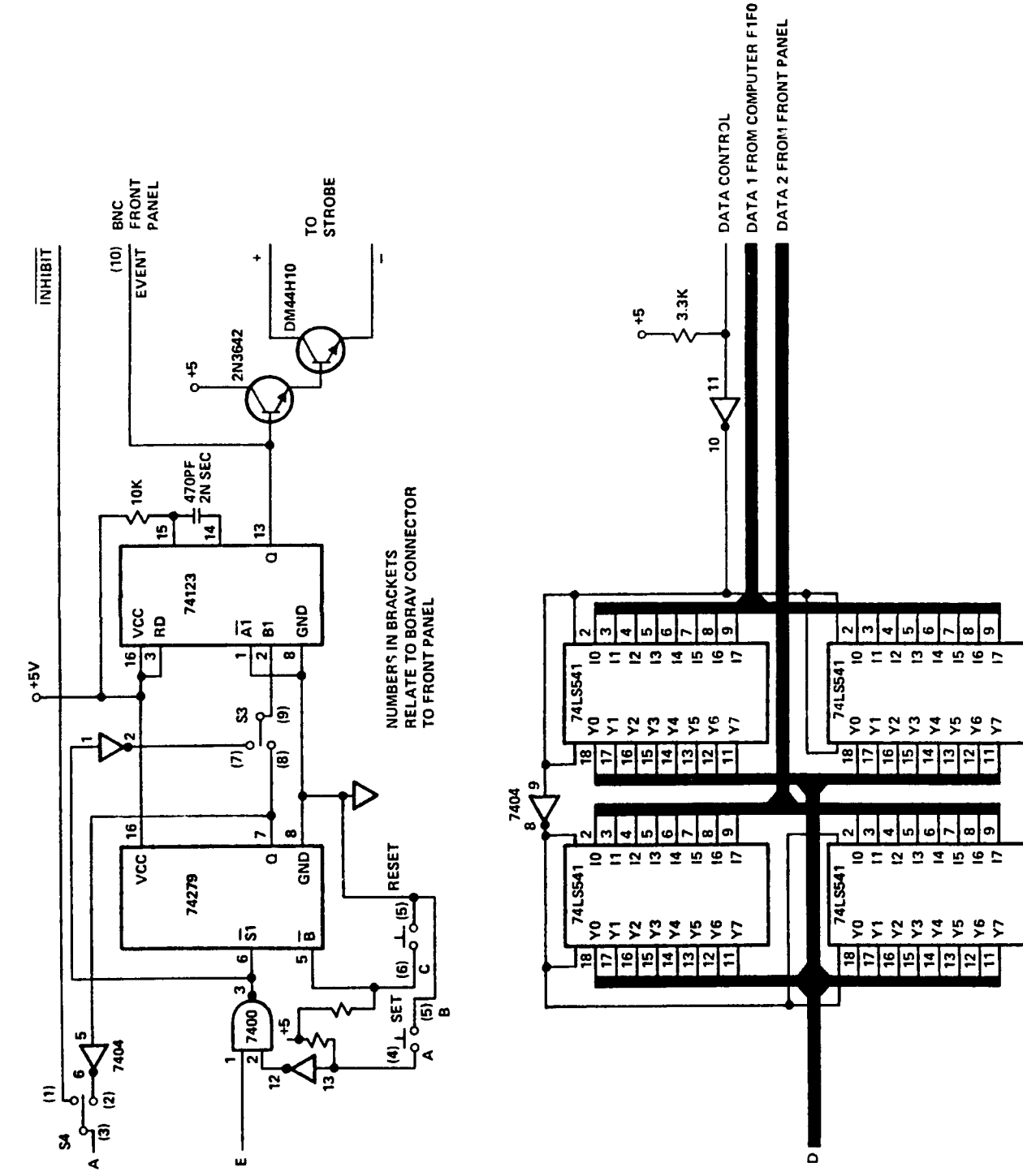


Fig. 3. Concluded.

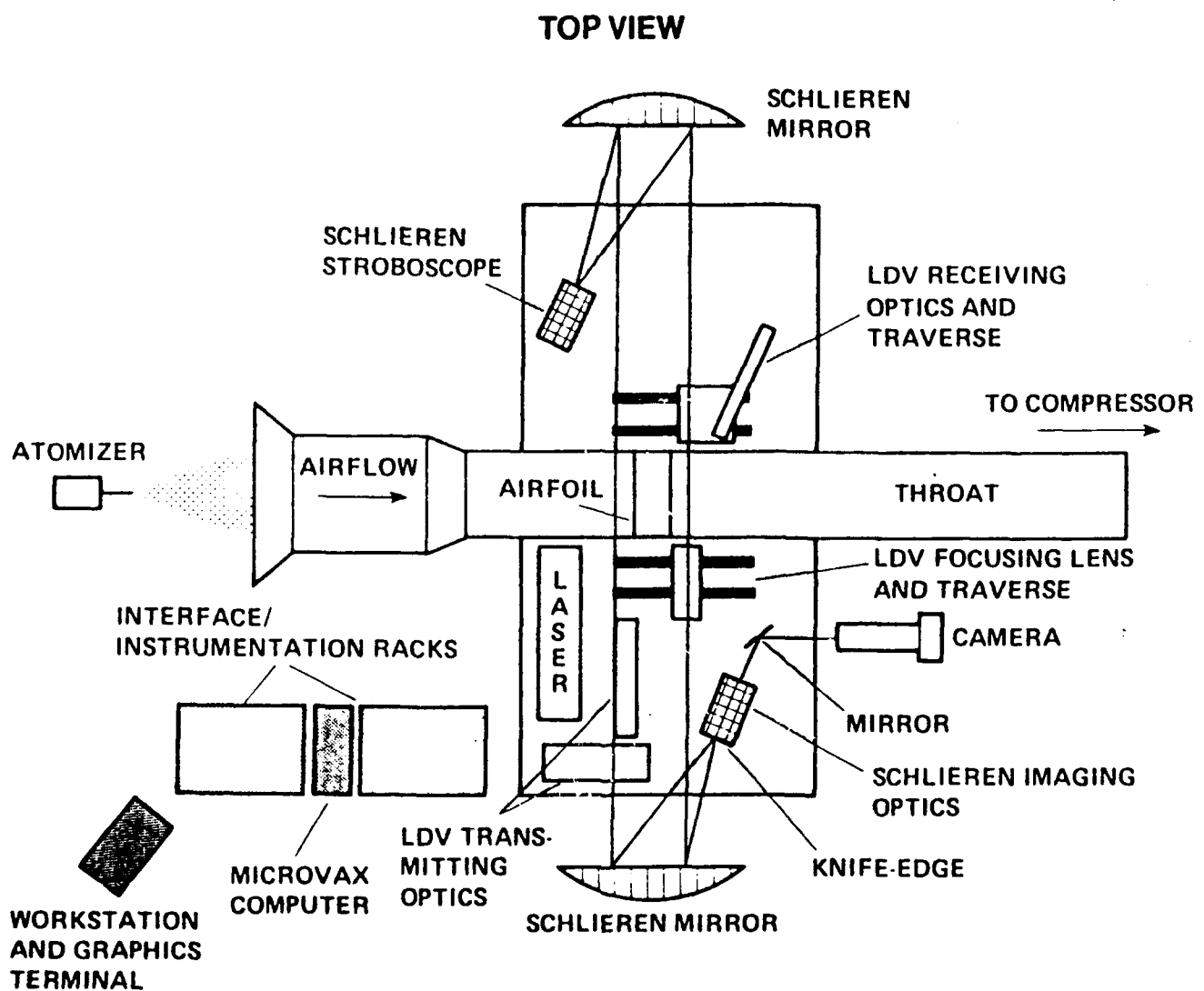


Fig. 4. Schematic of the CDSF Schlieren and LDV Instrumentation

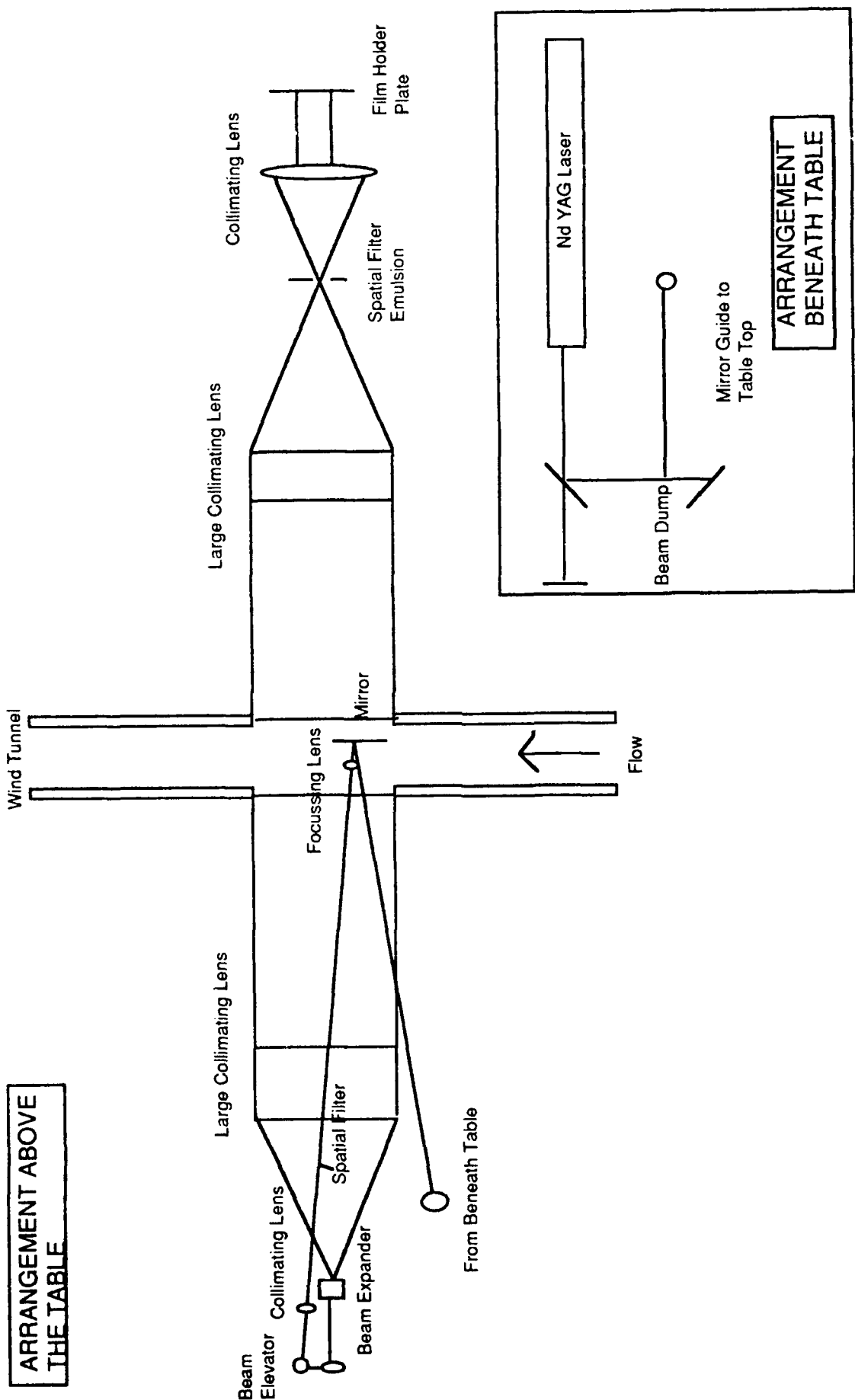


Fig. 5. Schematic of the Optical Arrangement of the Dark Center Interferometer System for the CDSF

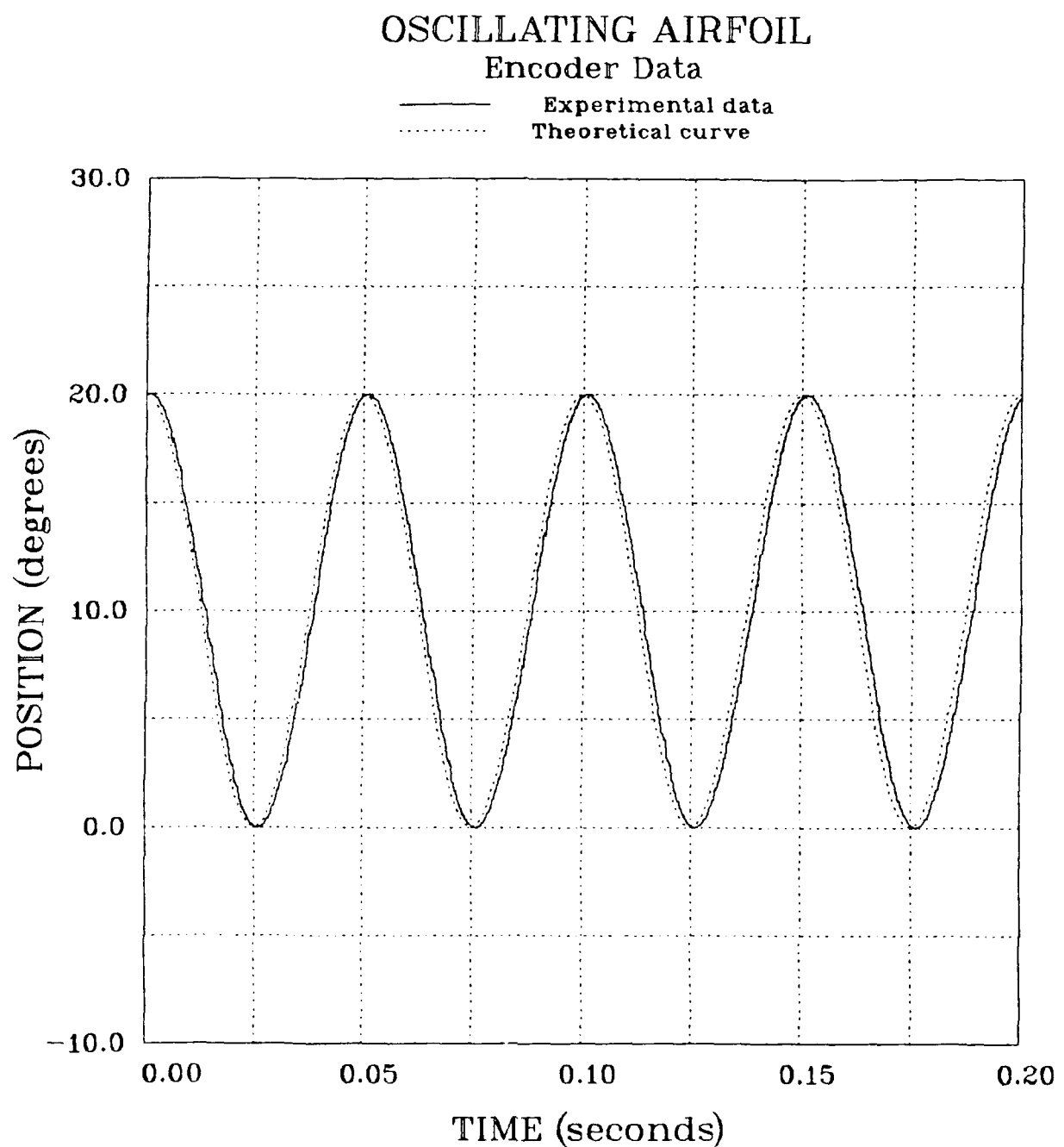


Fig. 6. Representative Calibration Data for the Oscillating Airfoil Drive:  $\alpha = 10^0 + 10^0 \sin \omega t$ ,  $f = 20$  Hz

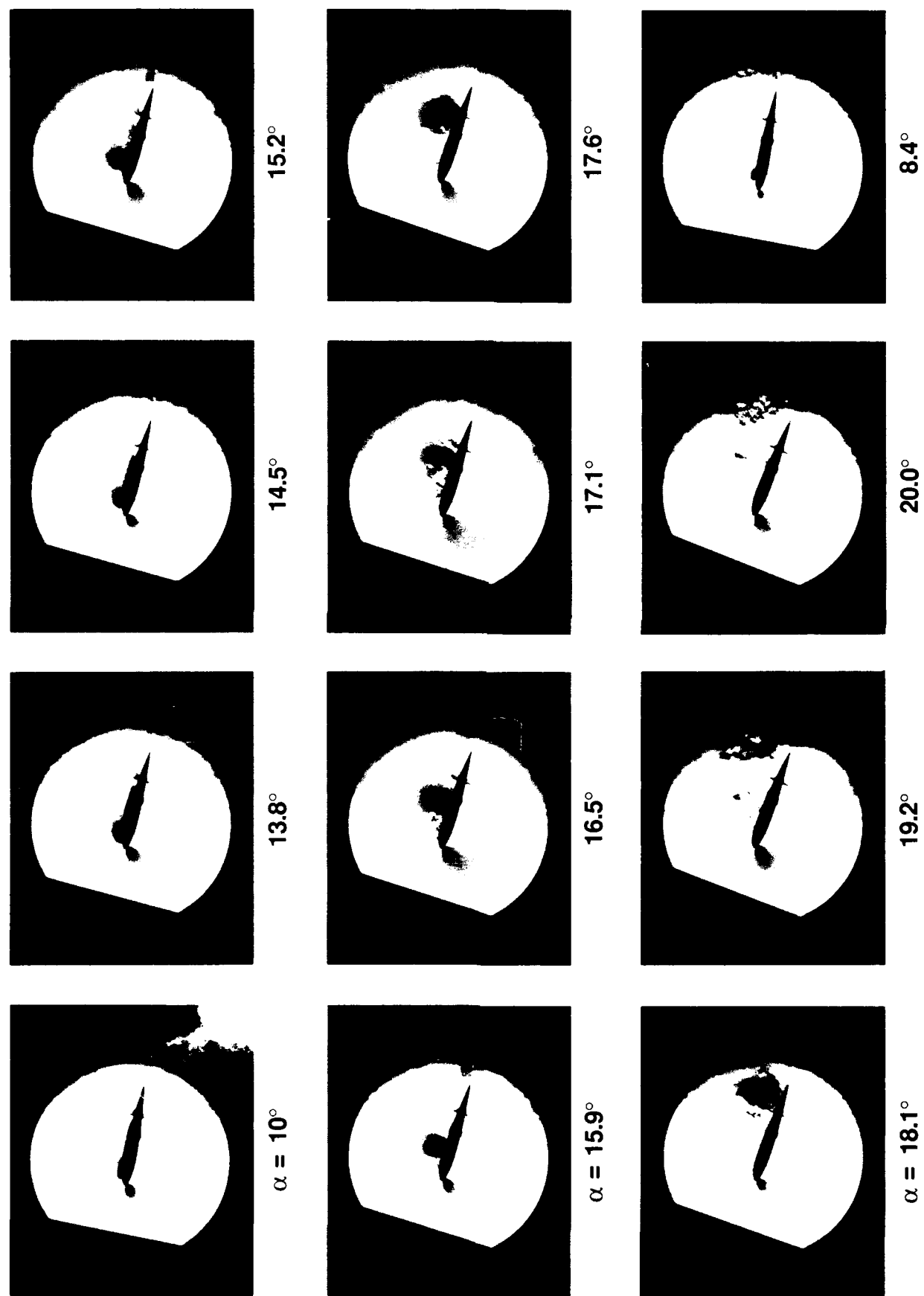


Fig. 7. Stroboscopic Schlieren Photographs of the Compressibility Effects on Dynamic Stall of an Oscillating Airfoil:  $M = 0.3$ ,  $k = 0.1$ ,  $\alpha = 10^\circ + 10^\circ \sin(\omega t)$

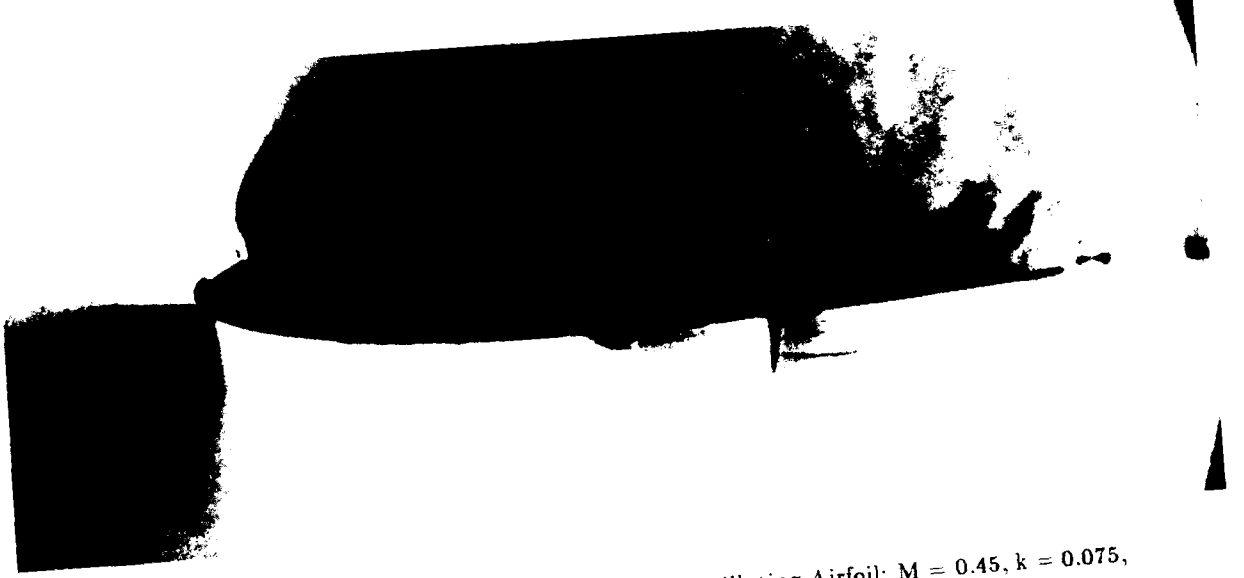


Fig. 8a. Schlieren Picture of Shock Over an Oscillating Airfoil:  $M = 0.45$ ,  $k = 0.075$ ,  
 $\alpha = 10^\circ + 2^\circ \sin \omega t = 9.1^\circ$

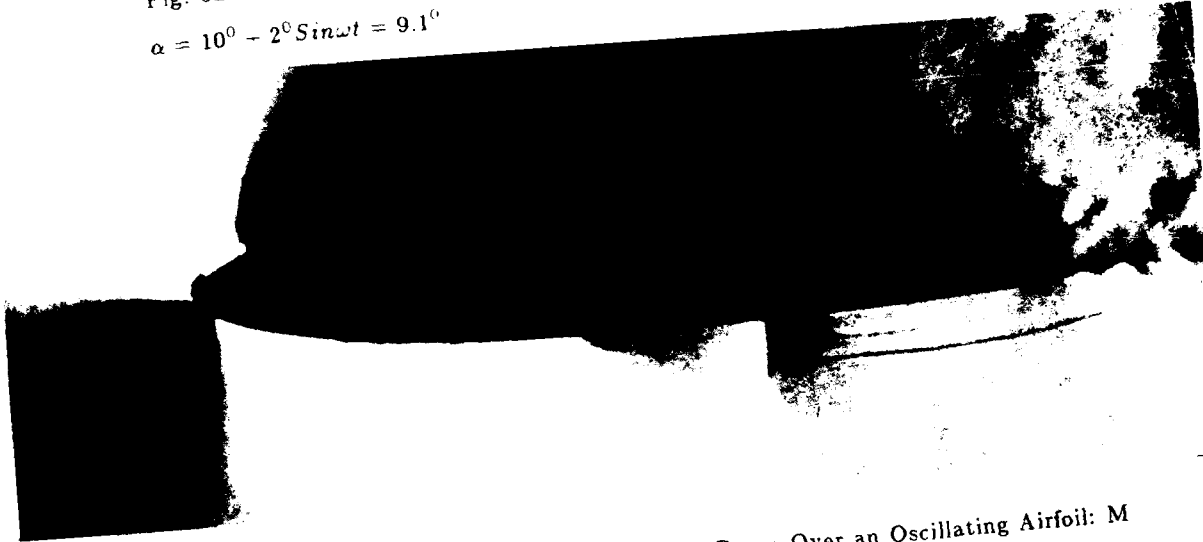


Fig. 8b. Schlieren Picture of Shock Breaking Down Over an Oscillating Airfoil:  $M$   
 $= 0.45$ ,  $k = 0.075$ ,  $\alpha = 10^\circ + 2^\circ \sin \omega t = 9.6^\circ$

SHOCK INDUCED SEPARATION (WHEN SHOCK  
HAS MOVED DOWNSTREAM)

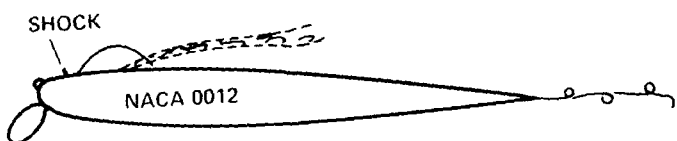


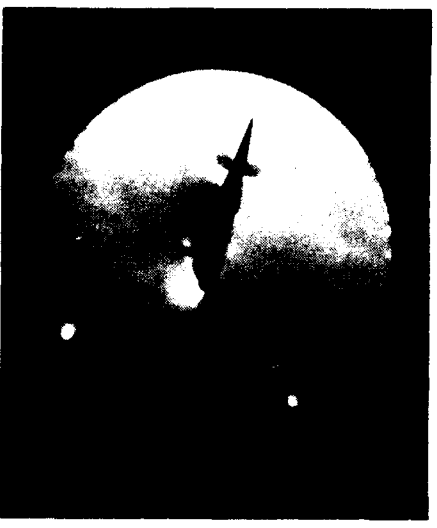
Fig. 8c. Schematic of Shock Induced Separation as Observed on Schlieren Image  
Plane



**M = 0.1**  
 $\alpha = 15.1^\circ$



**M = 0.2**  
 $\alpha = 15.1^\circ$



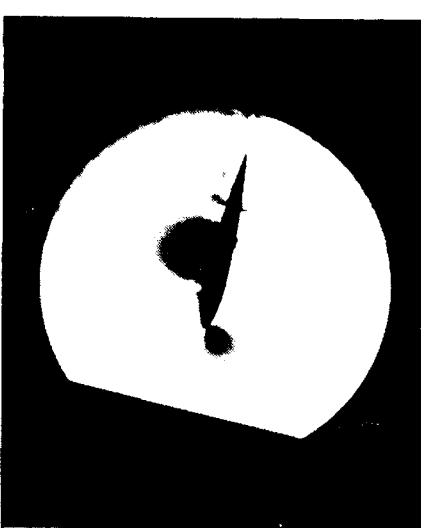
**M = 0.25**  
 $\alpha = 15.1^\circ$



**M = 0.35**  
 $\alpha = 13.8^\circ$



**M = 0.4**  
 $\alpha = 12.7^\circ$



**M = 0.45**  
 $\alpha = 12.3^\circ$

Fig. 9. Effect of Compressibility on Dynamic Stall of an Oscillating Airfoil:  $k = 0.05$

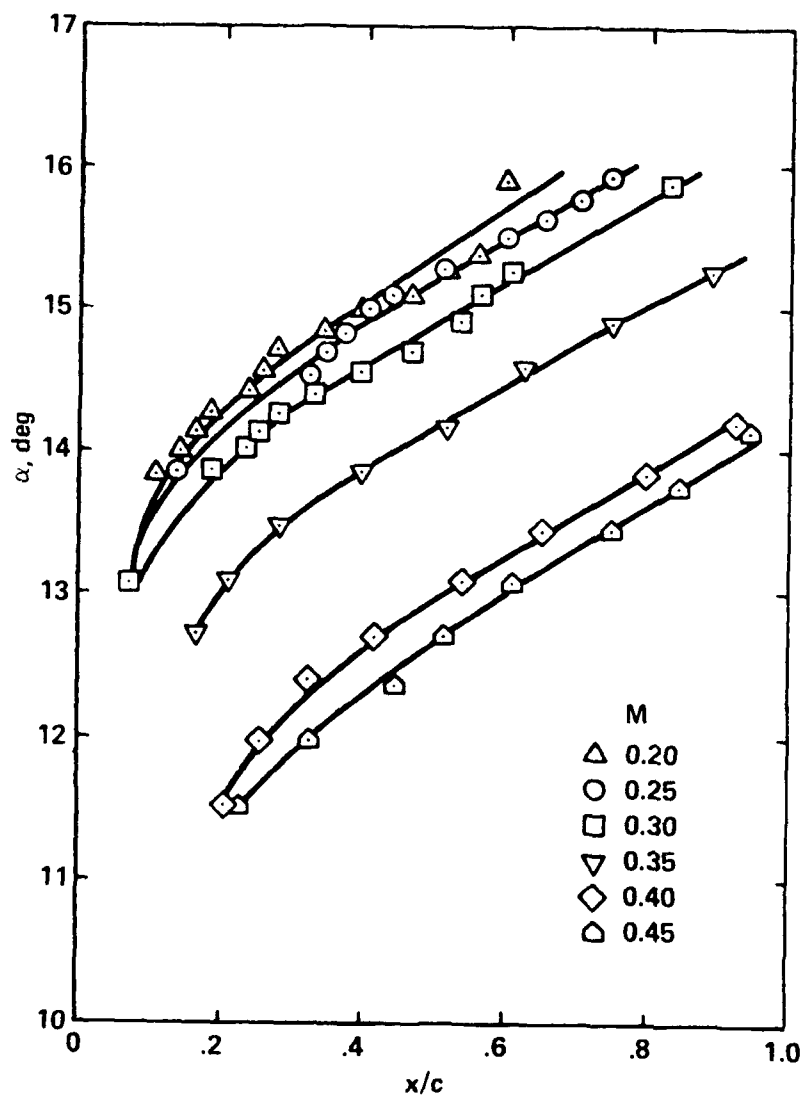


Fig. 10. Quantitative Effects of Mach Number on Dynamic Stall Process:  $k = 0.05$

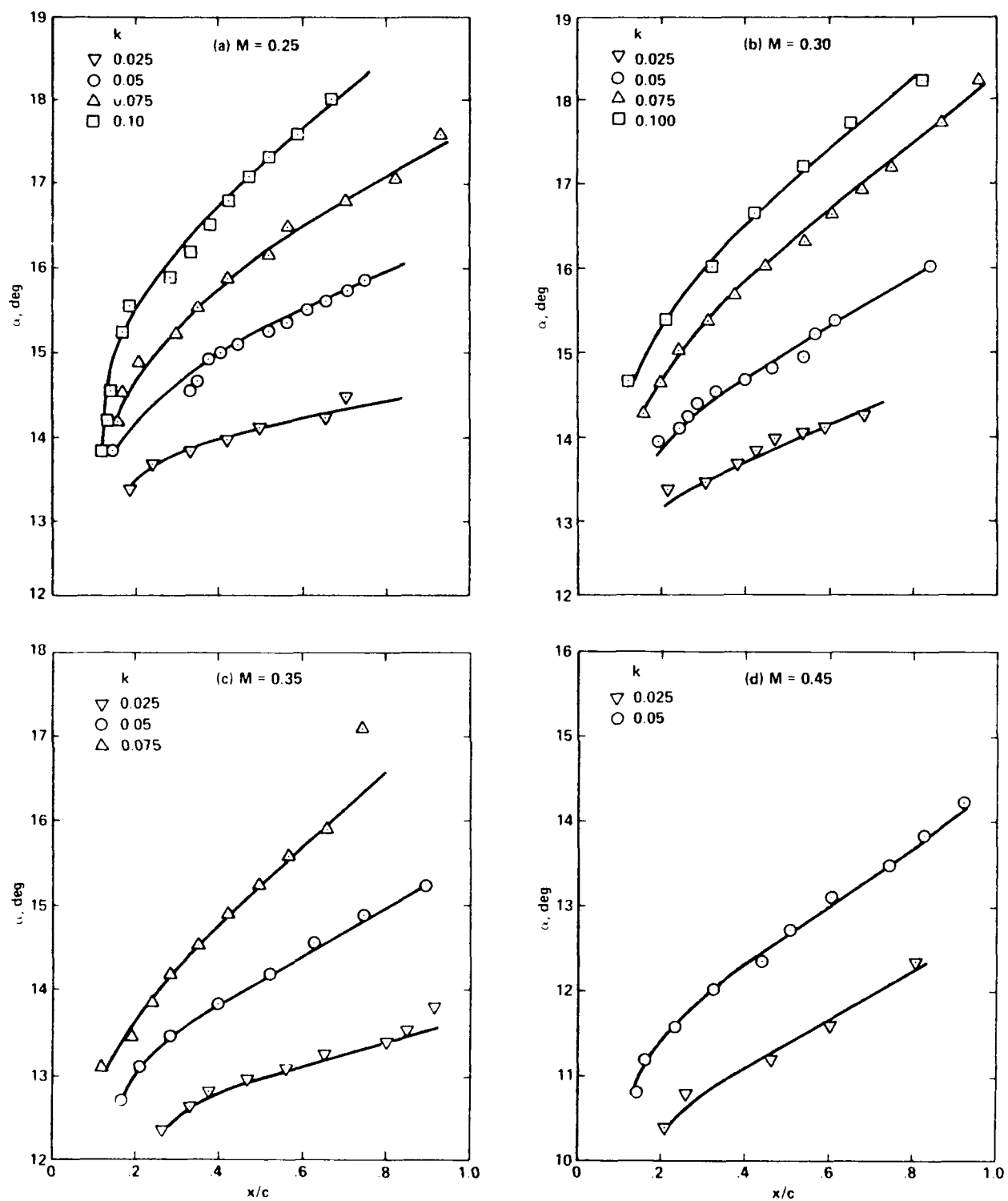


Fig. 11. Effects of Reduced Frequency on Dynamic Stall: (a)  $M = 0.25$ , (b)  $M = 0.3$ , (c)  $M = 0.35$ , (d)  $M = 0.45$ ,  $\alpha = 10^\circ + 10^\circ \sin \omega t$

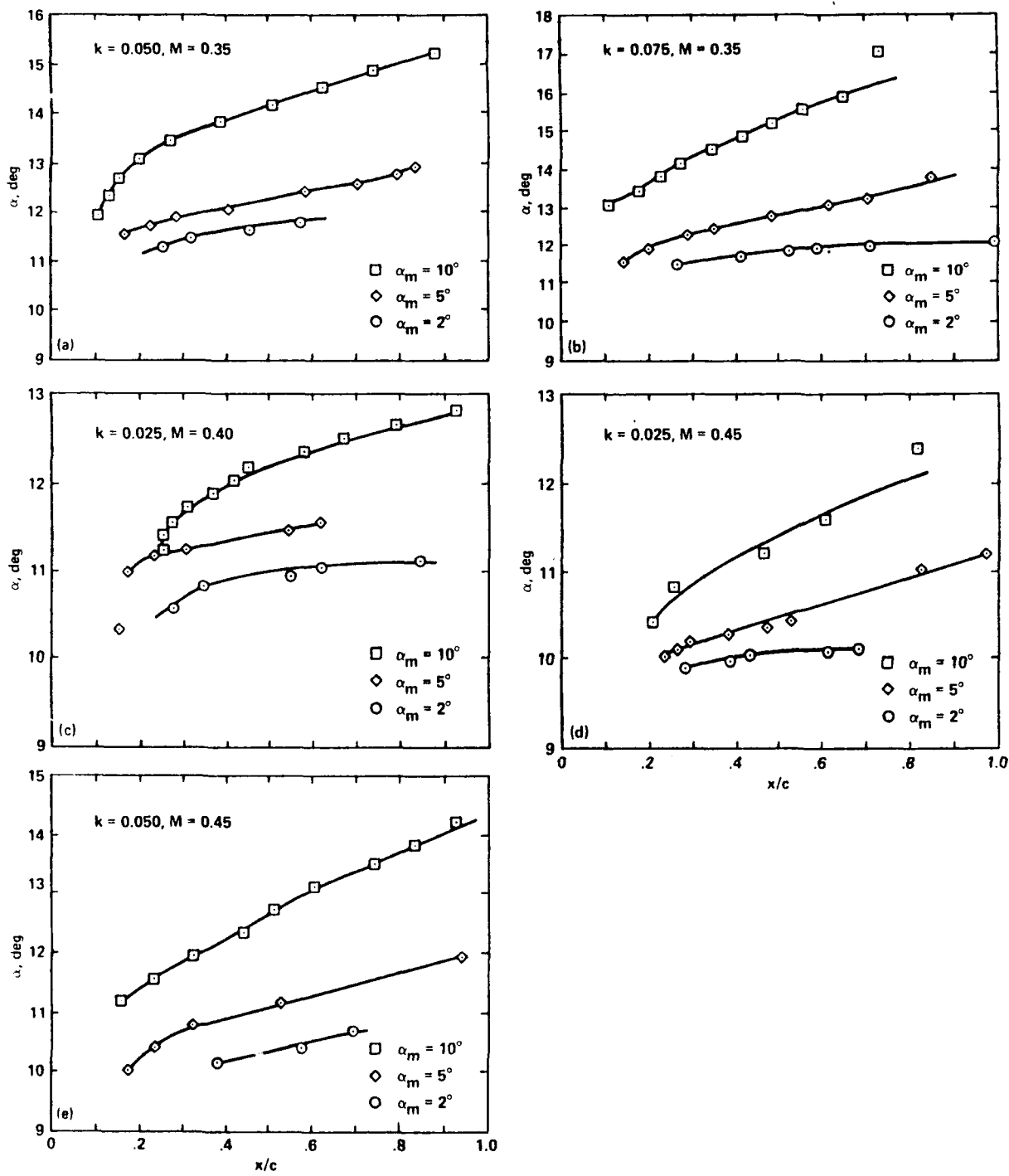


Fig. 12. Amplitude Effects on Dynamic Stall of an Oscillating Airfoil: (a)  $M = 0.35$ ,  $k = 0.05$ , (b)  $M = 0.35$ ,  $k = 0.075$ , (c)  $M = 0.4$ ,  $k = 0.025$ , (d)  $M = 0.45$ ,  $k = 0.025$ , (e)  $M = 0.45$ ,  $k = 0.050$ .



Fig. 13. Real-Time Interferogram of the Dynamic Stall Flow Over an Oscillating Airfoil:  $M = 0.45$ ,  $k = 0.05$ ,  $\alpha = 10^\circ + 10^\circ \sin \omega t = 10.32^\circ$ , (Inset shows details around the leading edge)

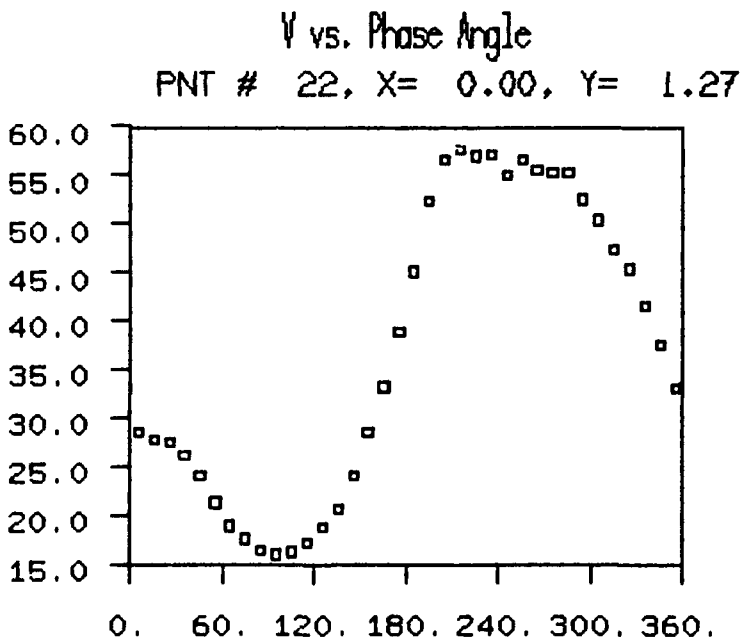
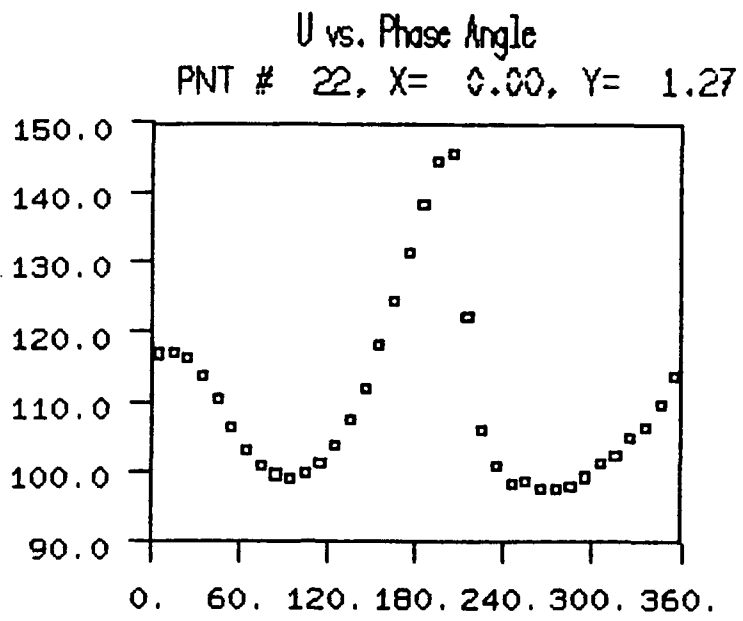


Fig. 14. Ensemble Averaged Velocities in the Flow Over an Oscillating Airfoil: LDV Data.  $M = 0.3$ ,  $k = 0.05$ ,  $x/c = 0.0$ ,  $y/c = 0.167$ ,  $z/c = 0.0$ ,  $\alpha = 10^\circ + 10^\circ \sin \omega t$